HEAT TRANSFER AUGMENTATION CHARACTERISTICS OF A FIN PUNCHED WITH CURVE TRAPEZOIDAL VORTEX GENERATORS AT THE REAR OF TUBES

by

Zhimin LIN*[*], *Zhaocheng WANG, Sha LI, Liangbi WANG, Yongheng ZHANG, Weiwei WANG, and Jing HE

School of Mechanical Engineering, Key Laboratory of Railway Vehicle Thermal Engineering of MOE, Lanzhou Jiaotong University, Lanzhou, Gansu, China

Original scientific paper
https://doi.org/10.2298/TSCI210827352L

The thermal-hydraulic characteristics of a novel fin punched with curve trapezoidal vortex generators (CTVG) are investigated numerically. The effects of multi-parameters including the geometry of CTVG, the location of CTVG, and working condition on thermal performance are considered. On one hand, CTVG can availably lessen the size of tube wake zone, decrease the mechanical energy consumption and heighten the fin heat transfer ability in this area. On the other hand, the secondary flow strength is strengthened because the longitudinal vortices generated by CTVG, which efficiently enhances the heat transfer on the fin downstream CTVG. Close relationship exists between the volume-averaged secondary flow strength and the mean Nusselt number. For studied cases, the optimal circumferential location angle of $\beta = 90^o$ is found, while the optimal radial location D_g is about 1.8 times the tube outside diameter. The smaller is the height or base length of CTVG, the better the thermal performance of the enhanced fin punched with CTVG. Better thermal performance is achieved as the fin spacing is about 0.24 times the tube outside diameter.

Key words*: finned tube heat exchanger, heat transfer augmentation, CTVG, numerical simulation*

Introduction

Fin side heat transfer augmentation technology is the most efficient measure to better thermal performance of finned tube heat exchanger. Many studies have shown that the reasonable organization of secondary flow generated by vortex generators (VG) can achieve a greater promotion of the heat transfer ability of the flow passage under the condition of small operating costs [1-3]. The application of VG is developed as an effective technique to control the secondary flow strength. Lots of work has been done in heightening the fin side heat transfer coefficient by using VG on fin surfaces [4-23]. For finned circular tube heat exchangers, the key point to improve the fin side thermal performance is to strengthen the local heat transfer ability and lessen the size of tube wake region, which are very closely dependent on the location and geometry parameters of VG.

As for the delta-winglet VG, there are many factors which influence the thermo-hydraulic characteristics. Lei *et al.* [4] and Lemouedda *et al.* [5] explored geometry parametric

[*] Corresponding author, e-mail: linzhimin@mail.lzjtu.cn

effects on fin side thermal performance including attack of angle, the aspect ratio of VG as well as tube arrangements. Chen *et al.* [6] applied winglet VG to oval tube bank fins, the function of VG in oval and flat tube bank fin is mainly to generate longitudinal vortices in comparison with the case of circular tube. Kim and Yang [7] studied rectangular channel with delta winglets on the lower surface, they found that in both common-flow down (CFD) and common-flow up (CFU) manners, the pair of vortices rotated in opposite directions, and the thermal performance for the case of CFD was better than that for CFU. Tiggelbeck *et al.* [8] had done the similar research on thermo-hydraulic performance for paralleled plates channel with punched delta winglets, and found that the performance of aligned delta winglet double rows was better than staggered one. Chen *et al.* [9] extended their work to multiple rows of in-line and staggered manners of VG manufactured in finned oval tube heat transfer elements. Unlike the staggered arrangement of VG in the study of Tiggelbeck *et al.* [8], the staggered VG in Chen's study [9] was placed in zigzag way, the tips of VG in each column pointed to the adjacent oval tubes. Compared with in-line manner of VG, Chen *et al.* [9] found that the overall thermal performance for staggered was superior to in-line arrangement. Wang [10] numerically studied the influences of six different arrangement of delta winglet VG, and found the optimal configuration is closely dependent on Re-values.

As for the rectangular VG, Naik and Tiwari [11] found that the location of VG is the dominant factor to affect the fin side thermal performance, and a superior heat transfer augmentation can be gained by placing rectangular VG to the upstream of each tube. Sarangi *et al.* [12] studied the enhanced heat transfer of an exchanger containing five inline rows of tubes and parallel fins with rectangular VG. They reported that the number of VG and their positional parameters have major effects on thermal performance. Gorji *et al.* [13] investigated the influence of the longitudinal location of rectangular winglet pairs on thermal-hydraulic characteristics at different Reynolds number. Their results showed that both Nusselt number and f go up as a result of the vortices strength augmentation. Leu *et al.* [14] obtained the optimized span angle of VG in the finned tube heat exchanger with inclined block shape VG.

Many other types of VG are mentioned in many literatures [15-23]. Dupont *et al.* [15] used embossed-type VG to generate secondary flow, their experimental research showed that the smooth embossed-type VG could enhance heat transfer ability for plate-fin exchangers. Another fin punched with interrupted annular grooves around circular tubes was investigated numerically in [16]. Recently, non-planar VG have been proposed by researchers. Gholami *et al.* [17] numerically studied the heat transfer augmentation performance by using wavy rectangular winglet VG. Zhou and Ye [18] used curve trapezoidal winglet type VG in rectangular cross-section channel and compared its thermal performance with rectangular, delta and trapezoidal winglet VG. Their results revealed that curve trapezoidal winglet VG had better thermal performance in fully turbulent zone. For practical engineering applications, a novel fin with curved winglet VG punched from and on the fin surface in the tube wake region is proposed [19-21]. Lin *et al.* [19, 20] and Gong *et al.* [21] performed the fin side thermal-hydraulic characteristics of a finned circular tube heat exchanger with curved delta-winglet and rectangular-winglet VG numerically, and their results indicated that this type of body fitted VG could play a favorable role in lessening the size of the tube wake. As expected, the enhancement of local heat transfer is dominated primarily by the geometry parameters of VG and their position [22, 23]. Although the wake reduction can be done by changing the tube shape [24], the feasibility and reliability to produce the heat exchanger using other shapes of tube is decreased greatly.

From aforementioned brief review it is found that the different shape of VG can improve heat transfer ability for some extent. Although different shapes of both plane and curve

VG used for improving the fin side thermo-hydraulic performance were widely investigated in many studies, there are few literatures to the fin with CTVG in the tube wake regions. For punched VG, they will cut the conduction paths in the fin along the circular tube radial direction, and the punched VG can enhance the heat transfer coefficient on the punched locations. Moreover, the punched VG will produce different vortex systems from the punched locations which may be related with the shape of VG. Thus, it is necessary to reveal the roles played by CTVG on thermo-hydraulic performance for continuation of our previous work topic. With the previous consideration, the thermal performance of the channel formed by four-row staggered tube bank fin punched with CTVG of multi-geometry parameter is numerically studied, and the parametric effects of CTVG under different flow conditions on Nusselt number and friction factor are considered to get their correlations.

Geometric description and mathematics formulation

Geometric description

Figure 1 is 3-D view of the finned staggered circular tube heat exchanger element with CTVG punched on the fins. In a real heat exchanger, as seen in fig. 2(a), circular holes and circular collars are stamped on the fin, by using expansion technology the tubes are contacted with a stack of parallel collared fins tightly, and the fin spacing is controlled by the circular flange. The CTVG pairs are stamped out at the rear region of each tube and are perpendicular to the fin having diameter of D_g around tube.

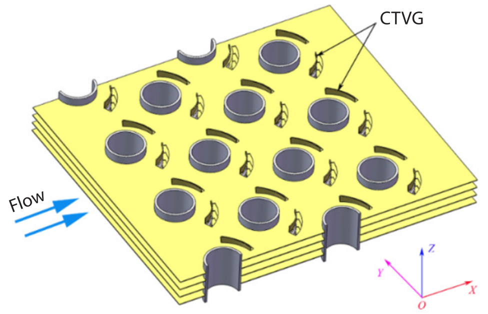

Figure 1. Finned circular tube exchanger with CTVG punched on fin surfaces

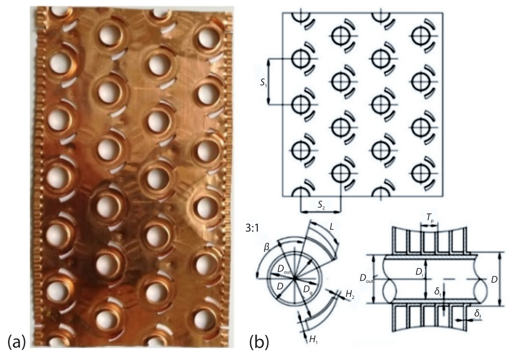

Figure 2. Fin geometry; (a) actual fin with CTVG and (b) geometrical parameters of CTVG

Figure 2(b) shows the position and geometry parameters of fin with CTVG. The parameters are indicated by the lateral tube distance, S_1, the longitudinal tube distance, S_2, the tube thickness, δ_t, the fin spacing, T_p, the fin thickness, δ_f, the tube inner diameter D_i, the height of VG facing upstream, H_1, the height of VG at the other end, H_2, the base length of VG, L, the base arc diameter of VG, D_g, and the angle, β, used to indicate VG radial and circumferential range, respectively. The calculation parameters are: $S_1 = 25.3$ mm, $S_2 = 22$ mm, $\delta_f = 0.15$ mm, $D = 9.0$ mm, $H_1 = 1.683$ mm. Three different $\beta = 90°$, $95°$ and $100°$, three different $D_g = 1.35D$, $1.55D$, and $1.75D$, three different $L = 3.5H_1$, $4.0H_1$, and $4.5H_1$, three different $H_2 = 0.2H_1$, $0.5H_1$, and $0.8H_1$, and three different $T_p = 0.211D$, $0.239D$, and $0.267D$ are considered to study the parametric effects of the novel fin with CTVG.

Due to the repetitiveness of tubes and CTVG pairs along transverse direction of the heat exchanger, the simulation region could be reduced as shown in fig. 3(a). The middle planes of the two adjoined fins are viewed as the bottom and top boundaries which make up the fluid-flow channel, the two base fins with the semi-thickness of fin and several holes. Thus, the inlet velocity is not uniform, and the temperature of the base fins at the inlet is unknown. To represent the actual flow with entrance boundary conditions, the calculation region is lengthened one time longitudinal tube distance upstream.

Mathematics formulation

The developed numerical model is based on the following assumptions:

– the physical property parameters are constant,
– the fluid is incompressible and the laminar flow and heat transfer are in steady-state, and
– in energy equation the viscous dissipation term is not considered.

Mass conservation equation:

$$\frac{\partial}{\partial x_i}(\rho u_i) = 0 \tag{1}$$

Momentum conservation equation:

$$\frac{\partial}{\partial x_i}(\rho u_i u_k) = \frac{\partial}{\partial x_i}\left(\mu \frac{\partial u_k}{\partial x_i}\right) - \frac{\partial p}{\partial x_k} \quad (k = 1, 2, 3) \tag{2}$$

Energy conservation equation:

$$\frac{\partial}{\partial x_i}\left(\rho c_{\mathrm{p}} u_i T\right) = \frac{\partial}{\partial x_i}\left(\lambda \frac{\partial T}{\partial x_i}\right) \tag{3}$$

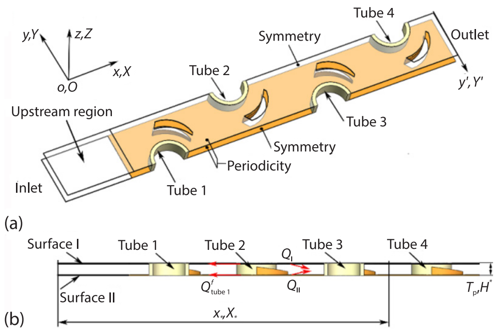

Figure 3. Simulation region; (a) simulation region and its solving constraints and (b) heat transfer balance through interfaces

The boundary conditions of the simulation domain are indicated in fig. 3(a). At the inlet, the bulk velocity is set to be u_{in}, the velocities in *y*- and *z*-direction are equal to zero, and the bulk temperature is set to be T_{in}, while at the outlet, the method proposed in [25] is adopted, for the details see [16, 19-21, 25]. On the two lateral sides of the simulation region, the symmetry boundary conditions are used for flow region, while for tube walls, the non-slipping condition for velocity and uniform temperature are used. On the top and bottom surfaces, there are three different boundaries, the symmetric conditions are used on the extended region surfaces; and the periodic conditions are used for core fin region, especially the non-slipping conditions used for velocity on the surface of the solid fin. The detailed description can be found in [16, 19-21].

To facilitate the application of the results, it is convenient to use non-dimensional forms. The dimensionless variables are expressed:

$$\begin{gathered} X = \frac{x}{D},\ Y = \frac{y}{D},\ Z = \frac{z}{D},\ U = \frac{u}{u_{\mathrm{in}}},\ V = \frac{v}{u_{\mathrm{in}}} \\ W = \frac{w}{u_{\mathrm{in}}},\ P = \frac{p}{\rho u_{\mathrm{in}}^2},\ N = \frac{n}{D},\ \Theta = \frac{T - T_{\mathrm{in}}}{T_{\mathrm{w}} - T_{\mathrm{in}}} \end{gathered} \tag{4}$$

The non-dimensional mathematics formulation can refer to our previous study [19, 20].

Formulas for data reduction

Reynolds number and Darcy friction factor:

$$\mathrm{Re}=\frac{\rho u_{\mathrm{in}} D}{\mu}, f=\frac{\Delta p D}{\frac{1}{2}\rho u_{\mathrm{in}}^{2} 4 S_{2}}=\frac{2\Delta p}{\rho u_{\mathrm{in}}^{2}} / \frac{4 S_{2}}{D}=\frac{2\Delta P}{L_{X}} \tag{5}$$

The local, span-averaged and overall-averaged Nusselt number is, respectively defined:

$$\mathrm{Nu}_{\mathrm{local}}=\frac{h_{\mathrm{local}} D}{\lambda_{\mathrm{f}}}=-\frac{\partial \Theta}{\partial N} /(\Theta_{\mathrm{fin}}-\Theta_{\mathrm{ref}}), \ \mathrm{Nu}_{\mathrm{s}}=\frac{\iint_{A_{x}} \mathrm{Nu}_{\mathrm{local}} \,\mathrm{d} A_{\mathrm{x}}}{\iint_{A_{x}} \mathrm{d} A_{\mathrm{x}}}, \ \mathrm{Nu}_{\mathrm{m}}=\frac{\iint_{A} Nu_{\mathrm{local}} \,\mathrm{d} A}{\iint_{A} \mathrm{d} A} \tag{6}$$

where the reference temperature $\Theta_{\mathrm{ref}} = (\Theta_{\mathrm{in}} + \Theta_{\mathrm{out}})/2$ is the same as introduced by Wang *et al.* [26].

To facilitate the description of secondary flow strength, the parameter, *Se*, is introduced [27]:

$$Se=\frac{\rho D^{2}|\Omega_{x}|}{\mu}=\frac{\rho D^{2}|\partial w / \partial y-\partial v / \partial z|}{\mu}=\mathrm{Re}\left|\frac{\partial W}{\partial Y}-\frac{\partial V}{\partial Z}\right| \tag{7}$$

Accordingly the span-averaged *Se*, (Se_{s}), and the overall averaged *Se*, (Se_{m}), are introduced:

$$Se_{\mathrm{s}}=\frac{\iint_{A_{x}} Se \,\mathrm{d} A_{x}}{\iint_{A_{x}} \mathrm{d} A_{x}}, \quad Se_{\mathrm{m}}=\frac{1}{V} \iiint_{V} Se \,\mathrm{d} V \tag{8}$$

Calculation method of and its validation

Grid generation and numerical method

To ensure the accuracy of the positional and geometrical parameters of CTVG, the simulation region is divided into several zones to generate grid. The combination of the double boundary method [28] and the infinite interpolation method [29] is used to generate the preliminary mesh, and then by solving the Poisson equation improve the local mesh distribution. The grid system in the Cartesian co-ordinate system is given in fig. 4. The punched CTVG and the base fins are meshed with solid blocks by steps, as shown in fig. 4(c). Then the governing equations are discretized by adopting control volume method, and SGSD scheme proposed in [30] is employed for the convection terms, while the central difference scheme is for the diffusion terms. In the flow region, the SIMPLE algorithm was adopted to deal with the coupling of velocity and pressure [31]. To overcome the decoupling between them, the momentum interpolation is applied [32]. The treatment of solid domain of the fin and VG and the mentioned numerical methods are the same as in our previous study [33].

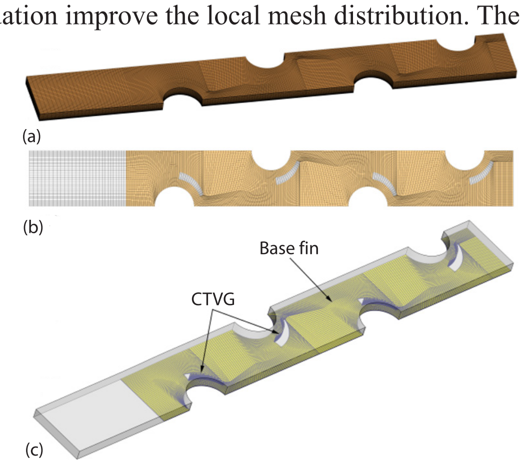

Figure 4. Grid system; (a) 3-D grid, (b) 2-D grid, and (c) CTVG and the fins

From fig. 3(b), if the calculation is fully converged, the total heat transfer rate transferred from the fins to the air and that transferred to the fins from the tubes should be identical on the basic of the thermal equilibrium relationship, thus the criteria of convergence for energy conservation equation can be defined:

$$\varepsilon = \frac{\left|\sum Q_{\text{tubei}}^{\text{f}} - Q_{\text{I}} - Q_{\text{II}}\right|}{\sum Q_{\text{tubei}}^{\text{f}}} \tag{9}$$

For all studied cases the relative error of $\varepsilon < 3\%$ is used.

Validations of grid independency and numerical method

Three different grid systems of 254 × 50 × 35, 302 × 55 × 41, and 350 × 65 × 48 are designed for grid independency test under the conditions of Re = 2000, $\beta = 95°$, $D_g = 1.35D$, $L = 4H_1$, $H_2 = 0.5H_1$, and $T_p = 0.239D$. The effects of grid number on Nu_m and f are listed in tab. 1. The differences of Nu_m and f are less than 3% for these three grid systems, in terms of accuracy and time cost the grid of 302 × 55 × 41 is used. In calculation, the grid size for various fin geometries was slightly adjusted. After the grid independency validation, the fin side thermo-hydraulic performance of finned staggered circular tube heat exchanger with punched CTVG was numerically and experimentally investigated to validate the reliability of the numerical method. Considering the laminar model used in this study, the maximum Reynolds number is limited by 3000. As shown in fig. 5, the trends of Nu_m and f with changing Reynolds number for numerical data and experimental ones of a real heat exchanger are the same in the overlapped range of Reynolds number. Based on the fitting data, we can obtain that when Reynolds number ranges from 1100-3000, the relative deviations of Nu_m and f ranges from 12.5-16.4% and 5.7-12.8% in comparison with experimental results, respectively. Considering the effects of multiple factors, the deviations are acceptable, and the present calculation results are reliable.

Table 1. Grid independency test

Grid numbers	Nu_m	f
254 × 50 × 35	28.296	1.212
302 × 55 × 41	28.381	1.191
350 × 65 × 48	28.961	1.189
Maximum error	2.01%	1.76%

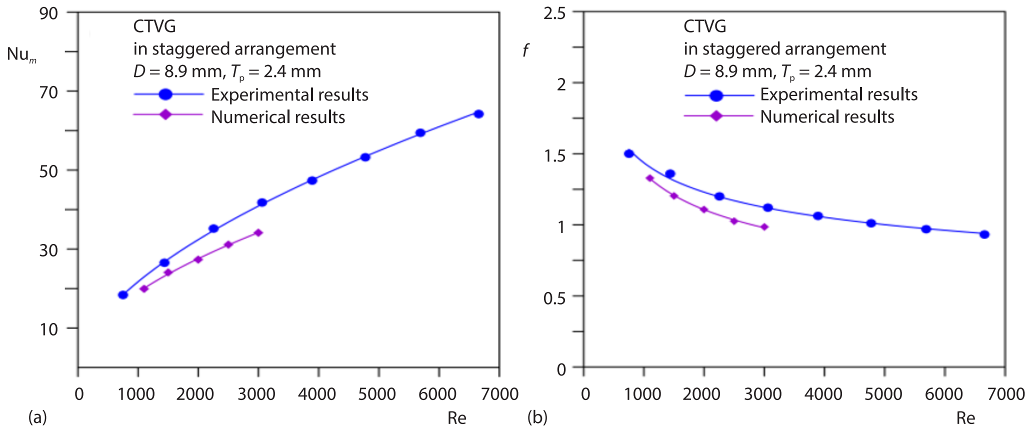

Figure 5. Numerical results validation; (a) Nu_m and (b) f

Discussions and analysis to the results

The reduction of the size of wake zone

A comparison of 3-D particle tracks in the passage with and without CTVG is given in fig. 6 when Re = 2000, $\beta = 95°$, $D_g = 1.35D$, $H_2 = 0.5H_1$, $L = 4H_1$, and $H^* = 0.239$. As seen in fig. 6(a), when air-flows across the tube, the flow separation near the rear of tube occurs and the trailing vortices is generated behind the tube for the plain fin geometry. While in the case with CTVG, as seen in fig. 6(b), one cannote that almost only flow separation appears from the tube wall and with less wake vortices when fluid-flows across the tube. When the fluid-flows across CTVG, nominally an accelerative flow channel beside downstream each tube would be formed by the tube and the side wall of VG, and this makes fluid-flow into the wake zone and then its size diminishes. Thus, on X-Y planes with the same location, the size of wake zone would be reduced and far smaller than the plain fin. The decrease in size of re-circulation zone is a favorable measure not only to reduce the mechanical energy dissipation, but also to promote the fin heat transfer ability behind each tube.

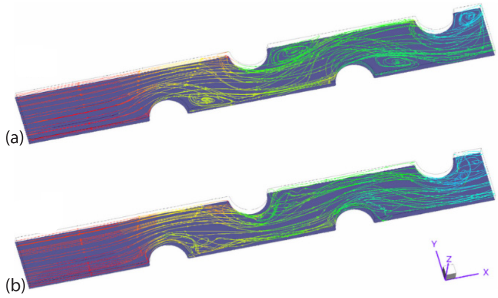

Figure 6. The 3-D particle tracks in the channel; (a) the plain fin and (b) the fin with CTVG

The heat transfer augmentation on the region behind the tube

Figure 7 presents the distribution of Nu_{local} on the upper and lower fin surfaces with and without CTVG at Re = 2000, $\beta = 95°$, $D_g = 1.35D$, $H_2 = 0.5H_1$, $L = 4H_1$, and $H^* = 0.239$. Because of the flow destabilization caused by CTVG, the flow characteristic close to CTVG are significantly different from the case without CTVG, thus the distribution of Nu_{local} on the fin surface are quite different to each other, especially behind CTVG as shown in figs. 7(a) and 7(b), Nu_{local} on Surface II is obviously higher than surface I. There is a large area behind the tube in which Nu_{local} is very low for the plain fin, but this area is decreased greatly in the case with CTVG. Immediately downstream CTVG, there is small area in which Nu_{local} is very large. Figure 7 clearly indicates that CTVG plays two roles to enhance heat transfer. The one is that CTVG lead to more fluid-flowing over the most part of the area behind the tube. The other one is that CTVG produce secondary flow, which can promote the mixing cold and hot fluids near-wall, and then enhance heat transfer locally.

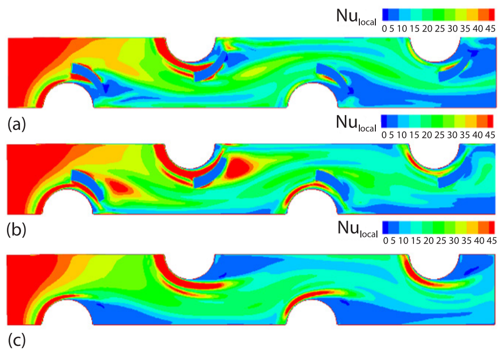

Figure 7. The Nu_{local} contours on fin surfaces; (a) and (b) the upper and lower fin surfaces of CTVG, respectively, and (c) the plain fin

The distributions of Nu_s in the main flow direction are expressed in fig. 8(a), Nu_s is very large at the front end of the fin, and then Nu_s decreases quickly. For the fin with CTVG, in the upstream of the first row tube, Nu_s gets a peak value on fin Surface II and then drops down along the main flow direction. Thanks to the action of the second row tube, Nu_s attains a peak value again when air-flows cross the second tube. Then Nu_s decreases rapidly and appears a minimum behind the circular tube. The aforementioned characteristics of Nu_s periodically arise

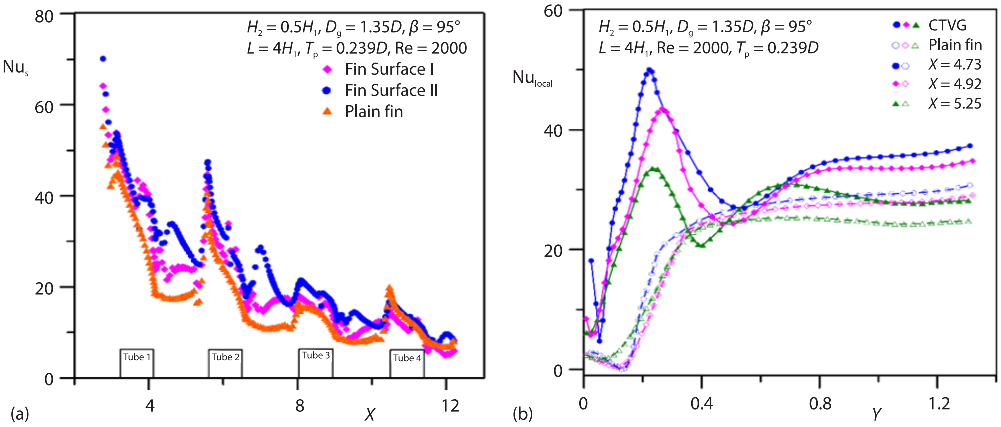

Figure 8. Changing trends of Nusselt number; (a) Nu_s in *X*-direction and (b) Nu_{local} on the lines of *X*= 4.73, *X*= 4.92, and *X* = 5.25

downstream every tube. At the front end of the first pair of CTVG, CTVG have limited impact on the flow structure, therefore, Nu_s are almost the same as that of the plain fin. Behind the first pair of CTVG, Nu_s on the upper fin surface are lower than that on the lower fin surface, and Nu_s on fin with CTVG are greater than that of the plain fin except the zone behind the fourth tube. Figure 8(b) presents the distributions of Nu_{local} at $X = 4.73$, $X = 4.92$, and $X = 5.25$ those are sequentially located just after the first row circular tube. The fluid temperature in the wake zones of the plain fin is fairly high, thus the heat transfer ability is weak in these re-circulation zones. While in the case with CTVG, due to CTVG located close to the tube, the wake regions are obviously reduced, and the low temperature mainstream fluid is guided towards tubes causing a better heat transfer. Thus, Nu_{local} behind the tube is greater than that of the plain fin. This indicated that Nu_{local} is affected significantly by CTVG, and the fin heat transfer ability behind the tube is obviously strengthened in the case with CTVG, which should be attributed to the enhanced secondary flow strength in the case with CTVG as illustrated later.

The enhancement of the secondary flow strength

Figure 9(a) describes the distribution of Se_s of the fin with or without CTVG. As seen in fig. 9(a), at the forefront of the tube, Se_s is the largest value for either the plain fin or the enhanced fin. For the plain fin, Se_s reduces smoothly downstream through to the coming of wake zone, and then Se_s raises smoothly get to the next forefront of the second row tube. For the fin with CTVG, Se_s reduces from the peak value located in the tube front stagnation point to the middle part of the tube, where Se_s reaches the smallest value, and then Se_s increases again because of CTVG on the fin surface. It is obviously that CTVG could increase the secondary flow strength efficiently. Figure 9(b) depicts the contrast of Se_m between the plain fin and the enhanced fin as Reynolds number varies from 1100-3000. As seen in fig. 9(b), the secondary flow strength quantified by Se_m increases when Reynolds number raises, and the secondary flow strength with CTVG is prevail over the plain fin under the given Reynolds number, and the gap of Se_m between them augments when Reynolds number increases.

For all studied cases, the correlations of Nu_m and f with Se_m are obtained:

$$Nu_m = 0.8865 Se_m^{0.4071} \tag{10}$$

$$f = 8.7522 Se_{\mathrm{m}}^{-0.2302} \tag{11}$$

The maximum deviation between the original data and the correlation ones is under 10% and 15%, respectively, which means that $\mathrm{Nu_m}$ is closely associated with Se_m. It implies that the secondary flow strength is of important function improve thermo-hydraulic performance for the fin punched with CTVG.

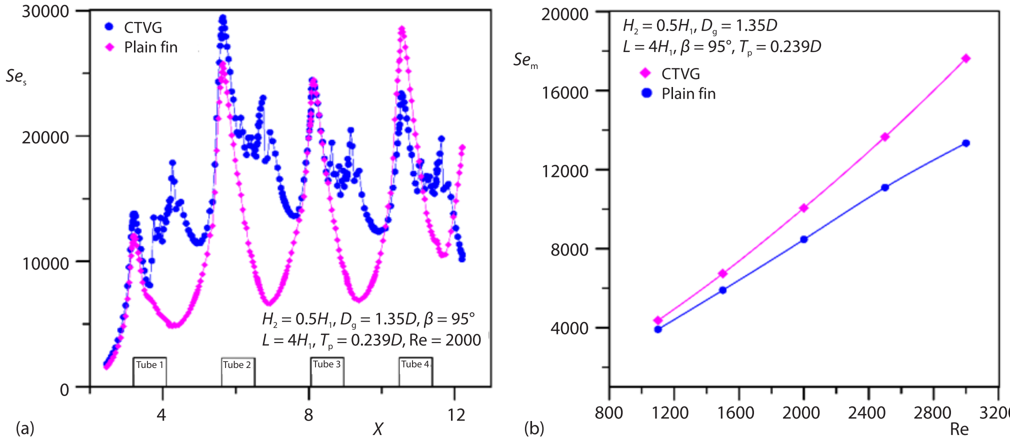

Figure 9. Comparison of the secondary flow strength between the referential plain fin and the enhanced fin with CTVG; (a) Se_s along X-direction and (b) Se_m as a function of Reynolds number

Comparative analysis of the thermal performance of CTVG and plain fin

The comparison of $\mathrm{Nu_m}$ and f between the plain fin and the fin with CTVG are presented in fig. 10 under identical Reynolds number anged from 1100-3000. The JF is the thermal performance factor under the same pumping power constraint, respectively:

$$JF = \frac{\dfrac{\mathrm{Nu_m}}{\mathrm{Nu_{m,ref}}}}{\left(\dfrac{f}{f_\mathrm{ref}}\right)^{1.3}} \tag{12}$$

The counterpart plain fin is chosen as a reference fin. As shown in fig. 10(b), JF is higher than 1.0 when Reynolds number ranges from 1100-3000, which indicates that CTVG could effectively improve the fin side thermal performance under the same pumping power constraint. As seen in fig. 10(b), JF increases with increasing Reynolds number, and which ranges from 1.15-1.26 for studied cases. It means that the fin with CTVG has more excellent thermal performance over the counterpart plain fin under the same pumping power constraint.

Parametric effects

The circumferential location of CTVG

Figure 11 depicts the influence of β on $\mathrm{Nu_m}$, f, and JF. As seen in figs. 11(a) and 11(b), $\mathrm{Nu_m}$ descends and f increases as β increases at a given Reynolds number. As seen in figs. 11(c), JF decreases when β increases, and JF increases with increasing Reynolds number at a given β. The thermal performance of CTVG becomes better when β is smaller. It implies that β is a significant parameter in fin design of CTVG. The studied cases of β = 90º could reach better thermal performance.

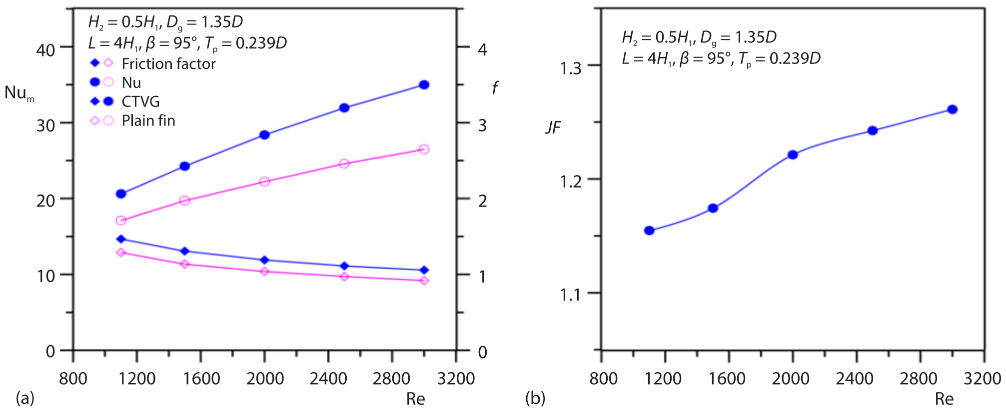

Figure 10. Comparison of thermal performance between the plain fin and the fin with CTVG; (a) Nu_m and f and (b) JF

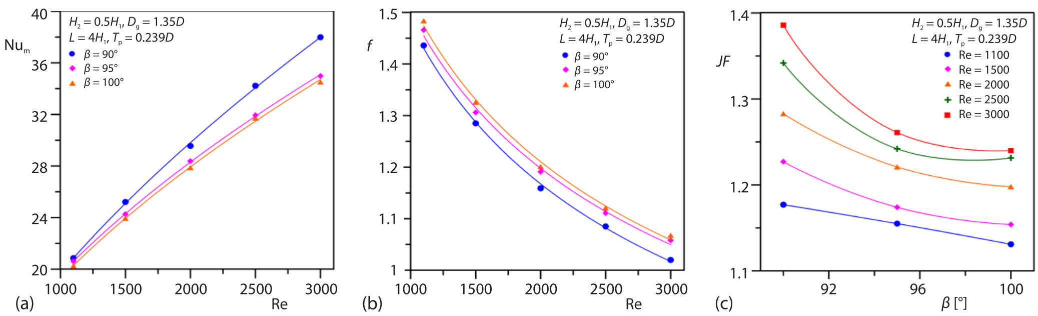

Figure 11. Influence of the circumferential location of CTVG; (a) Nu_m, (b) f, and (c) JF

The radial location of CTVG

Three different D_g/D = 1.35, 1.55, and 1.75 are used to ascertain the influence of the radial location of CTVG. As seen in figs. 12(a) and 2(b), both Nu_m and f increase when D_g/D increases at a given Reynolds number. It is found from fig. 12(c) that JF increases with increase of D_g/D. This implies that an excellent thermal performance of the enhanced fin with CTVG can be obtained when D_g/D is larger. These characteristics might be ascribed to that D_g/D determines the degree of CTVG to enforce the fluid-flowing into the wake region. If D_g/D is small, too much fluid is enforced into the wake region, although heat transfer is enhanced, the pressure loss is large. If D_g/D is large, too little fluid is enforced into the wake region, and the pressure loss is small, but the heat transfer augmentation is also weak. Thus, D_g/D is of important function enhance heat transfer of the fin punched with CTVG. The D_g/D is larger in the scope of this study, the thermal performance is better.

The base length of CTVG

As seen in figs. 13(a) and 13(b), Nu_m descends and f increases as the base length increases for a given Reynolds number. As seen in fig. 13(c), JF decreases with increasing the base length. As indicated by JF, the thermal factor of the enhanced fin with CTVG excelled when the base length is smaller. The main reason is that large base length would cut more paths of the fin thermal conduction, and thus weaken the fin heat transfer ability; on the other hand the larger base length would lead to higher pressure drop.

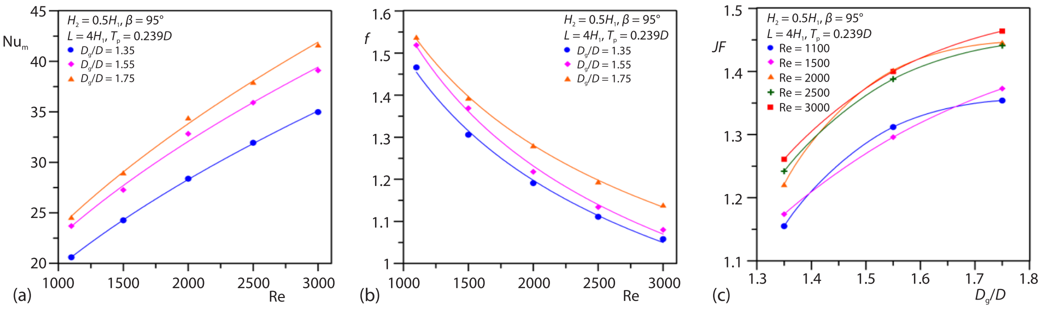

Figure 12. Influence of the radial location of CTVG; (a) Nu$_m$, (b) *f*, and (c) *JF*

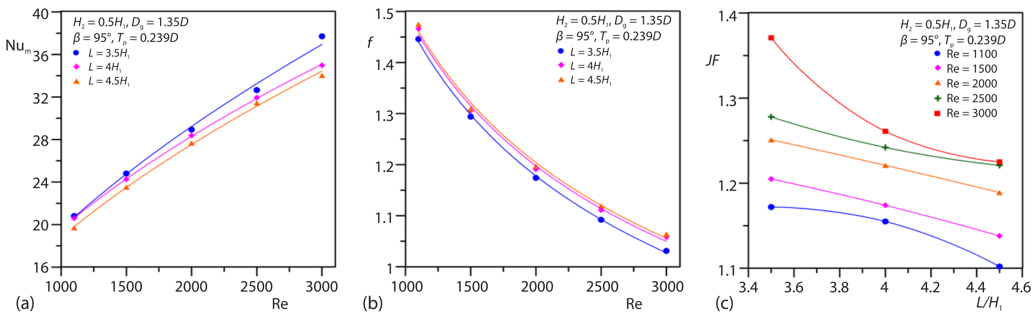

Figure 13. Influence of the base length of CTVG; (a) Nu$_m$; (b) *f*, and (c) *JF*

The edge height of CTVG

Figure 14 shows the influences of H_2/H_1 on Nu$_m$, f, and JF. As seen in figs. 14(a) and 14(b), Nu$_m$ descends and f increases with the increasing H_2/H_1 at a certain Reynolds number. In fig. 14(c), JF decreases with increasing H_2/H_1. It shows that CTVG with lower H_2/H_1 could efficiently improve thermal performance. These characteristics may be resulted from that H_2/H_1 determines the amount of air directed into the wake zone by CTVG. If H_2/H_1 is small, less fluid is flowed into the wake region, heat transfer is enhanced, and the friction loss is relatively smaller. If H_2/H_1 is large, more fluid is flowed into the wake region, which results in

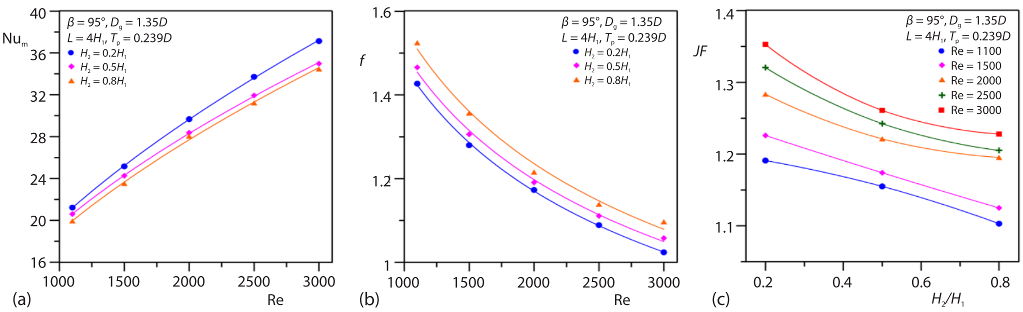

Figure 14. Influence of the edge height of CTVG; (a) Nu$_m$, (b) *f*, and (c) *JF*

enhancing heat transfer but with larger friction loss, and the friction loss penalty takes over the heat transfer augmentation. Thus, the edges height of CTVG is also a vital parameter to affect the fin heat transfer ability.

The fin spacing

Figure 15 shows the influence of the fin spacing H^* on $\mathrm{Nu_m}$, f, and JF. As shown in figs. 15(a) and 15(b), for the cases with CTVG, both $\mathrm{Nu_m}$ and f decrease when H^* is increased at a given Reynolds number. To judge the thermal performance at different fin spacing, JF defined by Hu *et al.* [34] is used:

$$JF = \frac{h}{h_{\mathrm{ref}}}\frac{u_{\mathrm{max,ref}}}{u_{\mathrm{max}}}\left(\frac{f_{\mathrm{ref}}}{f}\right)^{1/3}\left\{\frac{[1-\delta/(T_{\mathrm{p}}+\delta)]_{\mathrm{ref}}}{[1-\delta/(T_{\mathrm{p}}+\delta)]}\right\}^{1/3}\left[\frac{d_{\mathrm{e}}F}{(d_{\mathrm{e}}F)_{\mathrm{ref}}}\right]^{1/3}\left[\frac{(T_{\mathrm{p}}+\delta)_{\mathrm{ref}}}{T_{\mathrm{p}}+\delta}\right]^{1/3} \tag{13}$$

The plain fin with identical fin spacing is chosen as a reference fin. As seen in fig. 15(c), JF is greater than 1.0, and this implied that the thermal performance is better by using CTVG. At the same fin spacing except $H^* = 0.267$, JF increases as Reynolds number increases. At the same Reynolds number, JF mostly heightens firstly and then decreases with increasing H^* changed from 0.211-0.267. Thus, there is optimal H^*. The effect of H^* on $\mathrm{Nu_m}$, and f is enforced by the relative edge height of CTVG, which would affect the mass of fluid enforced into the wake zone and the secondary flow produced by CTVG.

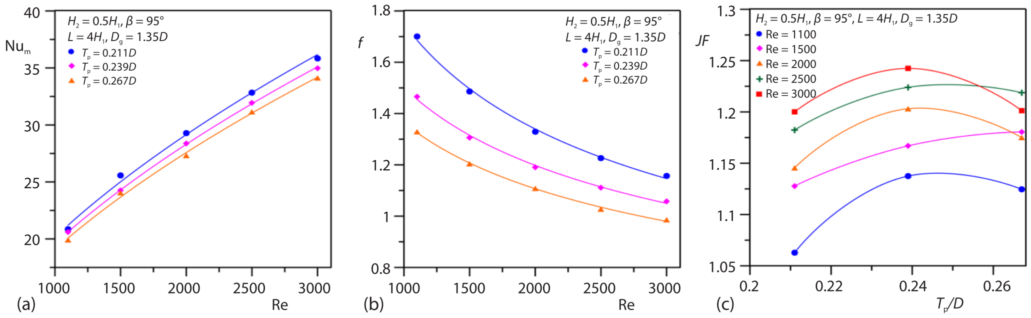

Figure 15. Influence of the fin spacing; (a) $\mathrm{Nu_m}$, (b) f, and (c) JF

The correlations between Reynolds number, $\mathrm{Nu_m}$, and f

The influences of Reynolds number, β, D_g, L, H_2, and T_p on thermal performance of the enhanced fin with CTVG are discussed together. To consider the overall effect of relevant parameters, the multiple non-linear regression analysis is used to get the formulas of $\mathrm{Nu_m}$ and f with Reynolds number, β, D_g, L, H_2 and T_p, respectively:

$$\mathrm{Nu_m} = 0.3336\mathrm{Re}^{0.5458}\left(\frac{\beta}{100}\right)^{-0.5945}\left(\frac{D_{\mathrm{g}}}{D}\right)^{0.7221}\left(\frac{L}{H_1}\right)^{-0.2299}\left(\frac{H_2}{H_1}\right)^{-0.0457}\left(\frac{T_{\mathrm{p}}}{D}\right)^{-0.2354} \tag{14}$$

$$f = 3.8814\mathrm{Re}^{-0.3325}\left(\frac{\beta}{100}\right)^{0.3311}\left(\frac{D_{\mathrm{g}}}{D}\right)^{0.2358}\left(\frac{L}{H_1}\right)^{0.0886}\left(\frac{H_2}{H_1}\right)^{0.0352}\left(\frac{T_{\mathrm{p}}}{D}\right)^{-0.8389} \tag{15}$$

where $1100 \le \mathrm{Re} \le 3000$, $90° \le \beta \le 100°$, $1.35 \le D_g/D \le 1.75$, $3.5 \le L/H_1 \le 4.5$, $0.2 \le H_2/H_1 \le 0.8$, $0.211 \le T_p/D \le 0.267$.

The fitness of eqs. (14) and (15) with numerical results is shown in fig. 16, and the maximum deviations of the fitting formula and the numerical results are almost less than 8% for Nu_m and f, respectively. Moreover, one cannote from eq. (14) that Reynolds number, and the radial location of CTVG have positive effect on Nu_m, while the other parameters have negative effect. Equation (15) shows that the main geometrical parameter that influences f is the fin spacing T_p.

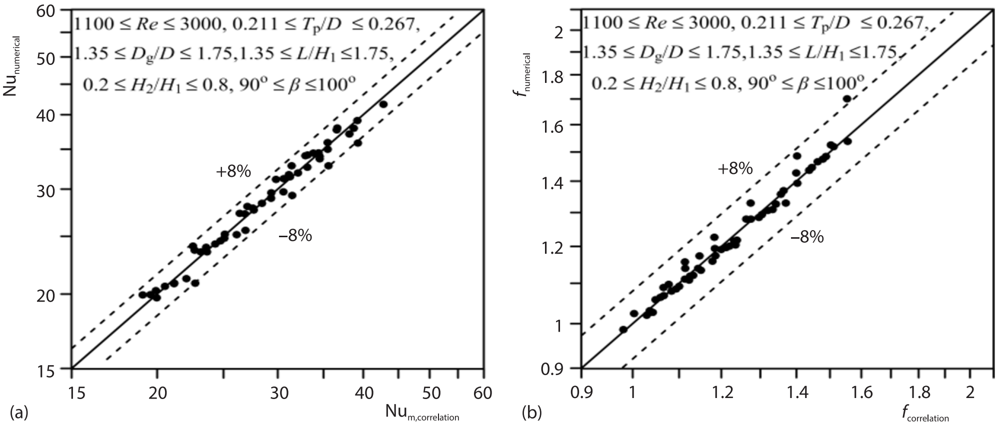

Figure 16. Comparisons of the numerical results with the correlations; (a) Nu_m and (b) f

Compared to the results in the related literature

In the investigations concerning with the heat transfer augmentation by curve rectangular VG (CRVG) and curve delta-winglet VG (CDWVG) used in finned circular tube exchanger, Gong *et al.* [21] and Lin *et al.* [19] found that both Nu_m and f are higher than that of the counterpart plain fin. Because the structure of exchanger studied in present paper is identical to their studied models except the shape of VG, thus the effects of the three different curve VG (CTVG, CRVG, and CDWVG) on the heat transfer ability are compared together. Figure 16 presents the comparisons of Nu_m, f, and *JF* for three different curve VG.

Figure 17(a) shows that for a given Reynolds number, Nu_m for the fin with VG are all prevail over that for the plain fin, and Nu_m are almost identical for three different curve VG. As seen in fig. 17(b), f in the presence of curve VG are all higher than that in the plain fin cases. The f in the case with CRVG is the largest and the difference of f in the two other cases with CTVG and CDWVG is small. To assess the optimal curve VG, the comparison of *JF* for the

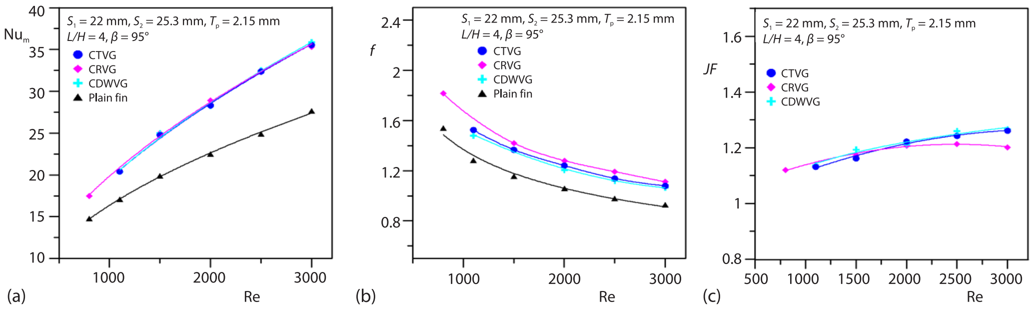

Figure 17. Comparisons with the results reported in the related literature; (a) Nu_m, (b) f, and (c) *JF*

three cases are presented in fig. 17(c). The *JF* for all the cases are greater than 1.0, which means that all of the three different curve VG effectively promote thermal performance in comparing with the counterpart fin geometry under the same pumping power constraint. When high Reynolds number is given, *JF* in the case with CRVG are the lowest, *JF* in the case with CDWVG are largest and the difference between CTVG case and CDWVG case is small. These show that the fin punching CTVG or CDWVG could obtain better comprehensive thermal performance in comparison with the fin punching CRVG.

Conclusions

A novel fin punched with CTVG behind the circular tube is proposed to improve the fin side thermal performance of exchanger. It is expected that CTVG can lessen the size of the re-circulation zone and produce the longitudinal vortices. To validate this expectation, the fin side flow and thermal characteristics is explored numerically. The investigation includes the influences of the geometric parameters of CTVG on the fi side thermal performance of the exchanger incorporated with circular tube bank fins. The main research findings are drawn as follows.

- The CTVG can efficiently lessen the size of wake zone through aiding fluid-flows into the wake zone. This could decrease the mechanical energy dissipation in the tube re-circulation zone, and strengthen the fin heat transfer ability in the wake zone.
- The CTVG can efficiently generate the longitudinal vortices. This would efficiently promote the heat transfer augmentation of the fin downstream CTVG.
- Close relationship exists between the dimensionless parameter describing the volume-averaged secondary flow strength and the mean Nusselt number. This indicates that the secondary flow strength strongly affects the fin side convective heat transfer for studied cases.
- The fin spacing and the geometrical parameters of CTVG, such as the radial location, the circumferential location, the base length and the edge height, affect the thermal performance of the fin punched with CTVG greatly. For the studied cases in this paper, the optimal circumferential location angle of $\beta = 90^{\circ}$ is found, while the optimal radial location Dg is about 1.8 times the tube outside diameter. The smaller is the base length or height of CTVG; the better is the thermal performance of the fin with CTVG. When the fin spacing is about 0.24 times the tube outside diameter, the better thermal performance could be obtained.
- The regression formulas of Nu_m and f with Reynolds number, β, D_g, L, H_2, and T_p are obtained.

Acknowledgment

This study was financially supported by the National Natural Science Foundation of China (51676093), the Gansu Provincial Foundation for Distinguished Young Scholars (1506RJDA061), Transformation of S&T achievements in Universities of Gansu Province (2018D-12), the Foundation of a Hundred Youth Talents Training Program of Lanzhou Jiaotong University, and Joint Innovation Foundation of Lanzhou Jiaotong University-Tianjin University (2018066).

Nomenclature

A – area of heat transfer surface, [m^2]
c_p – specific heat capacity, [kJkg^{-1}K^{-1}]
D – outside diameter including fin collar, [m]
D_g – curve winglet base arc diameter, [m]
f – Darcy friction factor, [–]
H_1 – long edge height of CTVG, [m]
H_2 – short edge height of CTVG, [m]
H^* – dimensionless fin spacing, (= T_p/D), [–]
h – heat transfer coefficient, [Wm^{-2}K^{-1}]
l – base length of CTVG, [m]

l_x – fin length, [m]
L_X – non-dimensional fin length, (= l_x/D), [–]
L – non-dimensional length of CTVG, (= l/D), [–]
n – local co-ordinates axis, [m]
Nu – Nusselt number, (= hD/λ), [–]
P – non-dimensional pressure, [=$p/(\rho u_{\text{in}}^2)$], [–]
Δp – dimensionless pressure drop, [–]
Q – heat transfer rate, [W]
Re – Reynolds number, (= $\rho u_{\text{in}}D/\mu$), [–]
S_1 – lateral tube distance, [m]
S_2 – longitudinal tube distance, [m]
Se – non-dimensional parameter of secondary flow strength, [–]
T_p – fin spacing, [m]
T – temperature, [K]
u_{in} – inlet velocity, [ms^{-1}]
u_i – velocity components, [ms^{-1}]
U_i – components of non-dimensional velocity vector, (= u_i/u_{in}), [–]
X_i – non-dimensional co-ordinates axes, (= x_i/D), [–]

Greek symbols

β – angle to indicate the circumferential location of CTVG [°]
δ – fin or tube thickness, [m]
ε – relative difference, [–]
λ – thermal conductivity, [Wm^{-1}K^{-1}]
μ – viscosity, [Pa·s]
ρ – density, [kgm^{-3}]
Θ – dimensionless temperature, [= $(T - T_{\text{in}})/(T_{\text{w}} - T_{\text{in}})$], [–]
Θ_{ref} – dimensionless average temperature, [= $(\Theta_{\text{in}} + \Theta_{\text{out}})/2$], [–]

Subscripts

f – fin surface
i – inner
in – inlet
I, II – fin surface I and II
local – local value
m – overall averaged
out – outlet
ref – reference
s – span-averaged
tubei – the i^{th} tube
w – tube wall

Superscripts

f – fin

References

[1] Fiebig, M., Vortex Generators for Compact Heat Exchangers, *Journal of Enhanced Heat Transfer*, *2* (1995), 1-2, pp. 43-61
[2] Jacobi, A. M., Heat Transfer Surface Enhancement Through the Use of Longitudinal Vortices: a Review of Recent Progress, *Experimental Thermal and Fluid Science*, *11* (1995), 3, pp. 295-309
[3] Ma, T., *et al.*, A Review on Thermoelectric-Hydraulic Performance and Heat Transfer Enhancement Technologies of Thermoelectric Power Generator System, *Thermal Science*, *22* (2018), 5, pp. 1885-1903
[4] Lei, Y. G., *et al.*, Hydrodynamics and Heat Transfer Characteristics of a Novel Heat Exchanger with Delta-Winglet Vortex Generators, *Chemical Engineering Science*, *65* (2009), 5, pp. 1551-1562
[5] Lemouedda, A., *et al.*, Optimization of the Angle of Attack of Delta-Winglet Vortex Generators in a Plate-Fin-and-Tube Heat Exchanger, *International Journal of Heat and Mass Transfer*, *53* (2010), 23, pp. 5386-5399
[6] Chen, Y., *et al.*, Conjugate Heat Transfer of a Finned Oval Tube with a Punched Longitudinal Vortex Generator in form of a Delta Winglet-Parametric Investigation of the Winglet, *Int. J. Heat Mass Transfer*, *41* (1998), 23, pp. 3961-3978
[7] Kim, E., Yang, J. S., An Experimental Study of Heat Transfer Characteristics of a Pair of Longitudinal Vortices Using Color Capturing Technique, *International Journal of Heat and Mass Transfer*, *45* (2002), 16, pp. 3349-3356
[8] Tiggelbeck, S., *et al.*, Experimental Investigations of Heat Transfer Enhancement and Flow Losses in a Channel with Double Rows of Longitudinal Vortex Generators, *International Journal of Heat and Mass Transfer*, *36* (1993), 9, pp. 2327-2337
[9] Chen, Y., *et al.*, Heat Transfer Enhancement of Finned Oval Tubes with Staggered Punched Longitudinal Vortex Generators, *International Journal of Heat and Mass Transfer*, *43* (2000), 3, pp. 417-435
[10] Wang, Y., Numerical Study of Hydrodynamics and Thermal Characteristics of Heat Exchangers with Delta Winglets, *Thermal Science*, *24* (2020), 1A, pp. 325-338
[11] Naik, H., Tiwari, S., Thermal Performance Analysis of Fin-Tube Heat Exchanger with Staggered Tube Arrangement in Presence of Rectangular Winglet Pairs, *International Journal of Thermal Sciences*, *161* (2021), Mar., pp. 106723-20
[12] Sarangi, S. K., *et al.*, Numerical Analysis of Thermofluid Performance of Fin-and-Tube Heat Transfer Surface Using Rectangular Winglets, *Journal of Heat Transfer*, *141* (2019), 10, pp. 101801-13

[13] Gorji, M., *et al*., Numerical Analysis on Longitudinal Location Optimization of Vortex Generator in Compact Heat Exchangers, *International Journal for Numerical Methods in Fluids*, *66* (2011), 6, pp. 705-713
[14] Leu, J. S., *et al*., Heat Transfer and Fluid-flow Analysis in Plate-Fin and Tube Heat Exchangers with a Pair of Block Shape Vortex Generators, *International Journal of Heat and Mass Transfer*, *47* (2004), 19, pp. 4327-4338
[15] Dupont, F., *et al*., Experimental Study of the Flow in a Compact Heat Exchanger Channel With Embossed-Type Vortex Generators, *Journal of Fluids Engineering*, *125* (2003), 4, pp. 701-709
[16] Lin, Z. M., *et al*., Numerical Study on Heat Transfer of Circular Tube Bank Fin Heat Exchanger with Interrupted Annular Groove Fin, *Applied Thermal Engineering*, *73* (2014), 2, pp. 1465-1476
[17] Gholami, A. A., *et al.*, Heat Transfer Enhancement and Pressure Drop for Fin-and-Tube Compact Heat Exchangers with Wavy Rectangular Winglet-Type Vortex Generators, *International Communications in Heat and Mass Transfer*, *54* (2014), May, pp. 132-140
[18] Zhou, G., Ye, Q., Experimental Investigations of Thermal and Flow Characteristics of Curved Trapezoidal Winglet Type Vortex Generators, *Applied Thermal Engineering*, *37* (2012), May, pp. 241-248
[19] Lin, Z. M., *et al*., Numerical Study of Flow and Heat Transfer Enhancement of Circular Tube Bank Fin Heat Exchanger with Curved Delta-Winglet Vortex Generators, *Applied Thermal Engineering*, *88* (2015), Sept., pp. 198-210
[20] Lin, Z. M., *et al*., Thermal and Flow Characteristics of a Channel Formed by Aligned Round Tube Bank Fins Stamped with Curve Delta-Winglet Vortex Generators, *Thermal Science and Engineering Progress*, *26* (2021), Dec., 101113
[21] Gong, B., *et al*., Heat Transfer Characteristics of a Circular Tube Bank Fin Heat Exchanger with Fins Punched Curve Rectangular Vortex Generators in the Wake Regions of the Tubes, *Applied Thermal Engineering*, *75* (2015), Jan., pp. 224-238
[22] Wang, Q., *et al*., Investigation on Heat Transfer Performance and Flow Resistance Characteristics in Finned-Tube Heat Exchangers With Different Vortex Generator Positions, *Journal of Heat Transfer*, *141* (2019), 9, pp. 091804-10
[23] Oh, Y., Kim, K., Effects of Position and Geometry of Curved Vortex Generators on Fin-Tube Heat-Exchanger Performance Characteristics, *Applied Thermal Engineering*, *189* (2021), May, pp. 116736-13
[24] Tala, J. V. S., *et al.*, Tube Pattern Effect on Thermal Hydraulic Characteristics in a Two-Rows Finned-Tube Heat Exchanger, *International Journal of Thermal Sciences*, *60* (2012), Oct., pp. 225-235
[25] Lin, Z. M., *et al*., A New Method to Specify the Outlet Boundary Condition of Fluid-flow in the Channel Formed by Tube Bank Fins, *Computational Thermal Sciences*, *3* (2011), 6, pp. 445-459
[26] Wang, L. C., *et al.*, The Characteristic Temperature in the Definition of Heat Transfer Coefficient on the Fin Side Surface in Tube Bank Fin Heat Exchanger, Numerical Heat Transfer – *Part A: Applications*, *60* (2011), 10, pp. 848-866
[27] Lin, Z. M., The Characteristics of Secondary Flow Heat Transfer Enhancement in Circular Tube with Twisted Tape or Vortex Generators (in Chinese), Ph. D. thesis, Lanzhou Jiaotong University, Lanzhou, China, 2011
[28] Eiseman, P. R., A Multi-Surface Method of Co-ordinate Generation, *Journal of Computational Physics*, *33* (1979), 1, pp. 118-150
[29] Eriksson, L. E., Practical Three-Dimension Mesh Generation Using Transfinite Interpolation, *SIAM J. Sci. Stat. Comp.*, *6* (1985), 3, pp. 712-741
[30] Li, Z. Y., Tao, W. Q., A New Stability-Guaranteed Second-Order Difference Scheme, Numerical Heat Transfer, *Part B: Fundamentals*, *42* (2002), 4, pp. 349-365
[31] Tao, W. Q., *Numerical Heat Transfer* (in Chinese), 2nd ed., Xi'an Jiaotong University Press, Xi'an, China, 2001
[32] Rhie, C. M., Chow, W. L., Numerical Study of the Turbulent Flow Past an Airfoil with Trailing Edge Separation, *AIAA J.*, *21* (1983), Nov., pp. 1525-1532
[33] Lin, Z. M., Wang, L. B., A Multi-Domain Coupled Numerical Method for a Flat Tube Bank Fin Heat Exchanger with Delta-Winglet Vortex Generators, Numerical Heat Transfer – *Part A: Applications*, *65* (2014), 12, pp. 1204-1229
[34] Hu, W. L., *et al*., The Optimum Fin Spacing of Circular Tube Bank Fin Heat Exchanger with Vortex Generators, *Heat and Mass Transfer*, *49* (2013), 9, pp. 1271-1285

Paper submitted: August 27, 2021
Paper revised: November 12, 2021
Paper accepted: November 15, 2021